SCIENTIFIC REPORTS

OPEN

SUBJECT AREAS:
POROUS MATERIALS
NANOSCALE MATERIALS

Received
23 September 2013

Accepted
28 October 2013

Published
13 November 2013

Correspondence and requests for materials should be addressed to J.L. (dr.linjing@gmail.com) or C.C.T. (tangcc@hebut.edu.cn)

Activated boron nitride as an effective adsorbent for metal ions and organic pollutants

Jie Li[1], Xing Xiao[1], Xuewen Xu[1], Jing Lin[1], Yang Huang[2], Yanming Xue[1], Peng Jin[1], Jin Zou[2] & Chengchun Tang[1]

[1]School of Materials Science and Engineering, Hebei University of Technology, Tianjin 300130, PR China, [2]Materials Engineering and Centre for Microscopy and Microanalysis, The University of Queensland, QLD 4072, Australia.

Novel activated boron nitride (BN) as an effective adsorbent for pollutants in water and air has been reported in the present work. The activated BN was synthesized by a simple structure-directed method that enabled us to control the surface area, pore volume, crystal defects and surface groups. The obtained BN exhibits an super high surface area of 2078 m^2/g, a large pore volume of 1.66 cm^3/g and a special multimodal microporous/mesoporous structure located at ~ 1.3, ~ 2.7, and ~ 3.9 nm, respectively. More importantly, the novel activated BN exhibits an excellent adsorption performance for various metal ions (Cr^{3+}, Co^{2+}, Ni^{2+}, Ce^{3+}, Pb^{2+}) and organic pollutants (tetracycline, methyl orange and congo red) in water, as well as volatile organic compounds (benzene) in air. The excellent reusability of the activated BN has also been confirmed. All the features render the activated BN a promising material suitable for environmental remediation.

Over the next couple of decades, the demand for fresh water and air will increase all over the world owing to population growth and industrial development. Effective removal of aqueous pollutant and toxic gas from the environment by taking advantage of new material and technique has always been a significant subject[1–3]. Adsorption is considered to be one of the simplest and most attractive methods for toxic gas, heavy metal ion and organic pollution purification. Activated carbon[4], magnetic hollow micropheres[5], carbonaceous nanofiber membranes[6], and aminated polyacrylonitrile fiber[7], have been proven effective for the absorption of the pollutants. However, the extraction of toxic gas and removal of aqueous pollutant in a safe and effective fashion still keep a technical challenge.

Porous boron nitride (h-BN) exhibits unique physical and chemical properties including high specific surface area, numerous structural defects, low density, high thermal conductivity, chemical durability, and oxidation resistance[8–10]. These features render porous BN material a promising candidate for applications in various fields, especially those related to adsorption like gaseous uptake, pollutant adsorption, and catalyst support[11–17]. For example, recent researches reported the interesting properties for dye and CO_2 adsorption in BN whiskers, nanotubes or nanosheets[18,19]. Porous BN microbelts and nanosheets with high specific surface areas are also reported as potential hydrogen storage media and valuable adsorbents for effective water cleaning, respectively[20,21]. Surface, defects, doping and porous nature in the structures play a crucial role in the adsorption of BN-based materials. Moreover, compared with the covalent C-C bond in the common used carbon-based adsorbents, the "lop-sided" densities characteristic of a considerable degree of ionic B-N bond makes the BN materials highly preferred for the absorption of the pollutants.

In this work we report a novel BN material, which we named as the activated BN, steming from the analogy of activated carbon, with the high efficient absorption for numerous pollutants in water and air. The activated BN can be defined as BN material with a high degree of porosity, an extended interparticulate surface area and high surface reactivity[22]. Compared with our previous work on porous BN[18], the novel activated BN was synthesized by a modified two-step process with the presence of P123 as a structure-directed agent. The simple method enabled us to control surface area, pore distribution, crystal defects and hydroxyl and organic surface groups. The synthesized activated BN possesses an extremely high surface area up to 2078 m^2/g, a special multimodal microporous/mesoporous structure located at ~ 1.3, ~ 2.7, and ~ 3.9 nm and abundant surface functional groups, which result in a fast and highly efficient adsorption of heavy metallic ions, toxic gas, and organic pollutants from the environments.

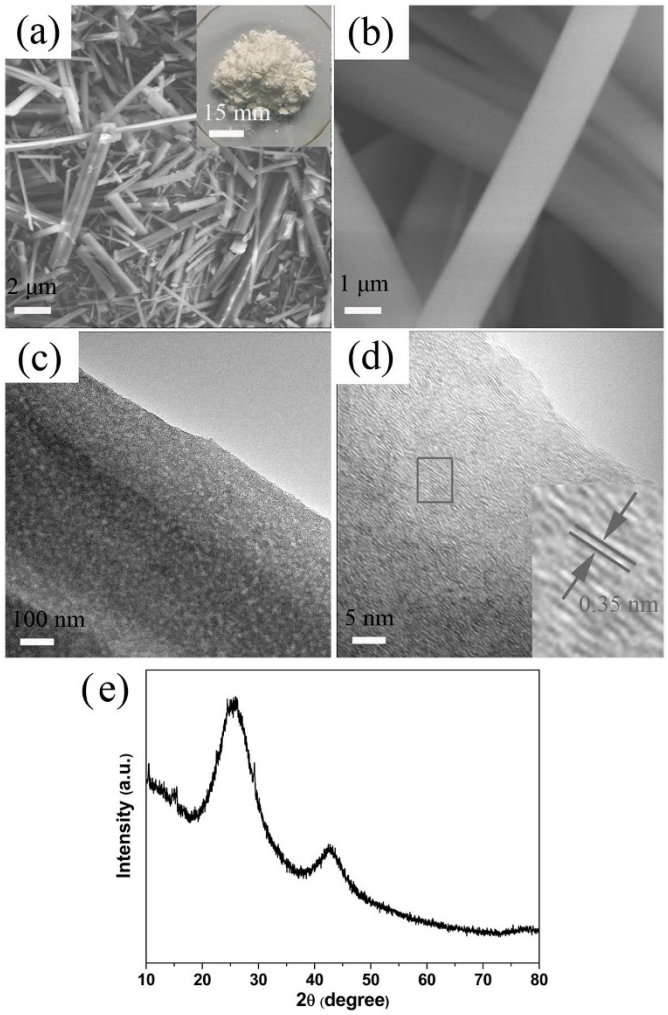

Figure 1 | (a) Low-magnification SEM image of the activated BN. (Inset) photographic image of the product. (b) The corresponding high-magnification SEM image. (c) TEM image of the ribbon-like activated BN. (d) Representative high-resolution TEM image. (e) XRD pattern of the activated BN.

Results

Characterization of activated BN. The activated BN is white in color and exhibits a ribbon-like microstructure with an average length of 80 μm, a thickness of 500 nm and a width of 1.0 μm, as displayed in Figure 1a,b. Transmission electron microscopy (TEM) observations reveal the presence of porous, rippled, and corrugated structure for all ribbons, a typical morphology as shown in Figure 1c. The inner layers interlink to form disordered cavities that are attributed to the porous geometry of the activated BN. The high-resolution TEM (Figure 1d) shows that the the activated BN consisted with layered BN of poor crystallization. A great number of defects, such as stacking faults exist on the surface, as shown in the inset of Figure 1d. In addition, the interspacing of the BN layers is ~ 0.35 nm, which is a little larger than that of the (002) fringes of bulk hexagonal BN[23]. The enlarged interspace has also been observed in the turbostratic BN materials[24], indicating their structural similarity. The structure of the product were also checked by X-ray powder diffraction (XRD). A broad peak around ~ 25.5° is observed, also indicating the poor crystallization of the layered BN with an the interplanar distances of around 0.35 nm. Figure 2 is the Fourier transform infrared (FTIR) spectrum of the as-synthesized activated BN. Compared with porous BN which we has reported in Ref. 18, the activated BN possesses richer surface bonds, such as B-OH/B-NH_2 (~3420, and ~ 3250 cm^{-1}), C=O (~1630 cm^{-1}), B-N(~1400 cm^{-1}), B-N-O (~1160 cm^{-1}), C-O (~1080 cm^{-1}), B-N-O (~930 cm^{-1}), and B-N-B(~800 cm^{-1})[25].

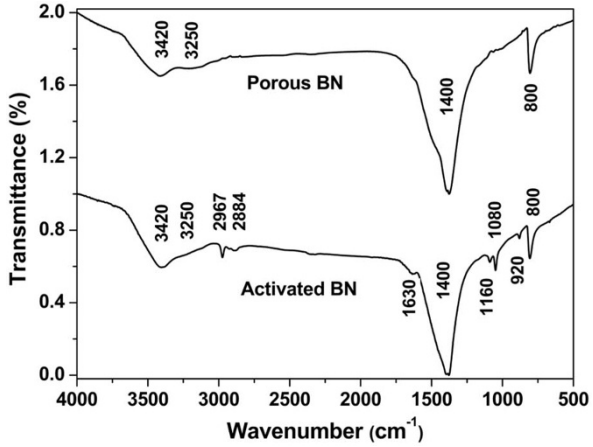

Figure 2 | **FTIR spectra of the activated BN and porous BN.**

Electron energy loss (EEL) spectroscopy and the element mapping techniques based on the energy-filtering TEM were adopted to analyze the compositional distribution of the activated BN. Figure 3a is an image obtained by using electrons with zero energy loss, displaying the porous structure of a micro-ribbon. Figure 3b is the corresponding EEL spectrum taken from the ribbon shown in Figure 3a. The EEL spectrum clearly shows the presence of the K-shell excitation shells of B (188 eV, B K-edge), N (401 eV, N K-edge), and O (532 eV, O K-edge), respectively. The sharp π^* and σ^* peaks of the B and N K-edges are typical for the sp^2 bonding configuration[26,27], which are characteristics of B-N layers. The quantification of the spectrum indicates a B/N composition ratio of ~ 1.1. The corresponding B and N elemental maps (Figure 3c and 3d) clearly indicate that the distributions of B and N are uniform and in consistent with the cavity distribution on the porous BN micro-ribbon. Oxygen (Figure 3e) indeed exists and also uniformly distributes over the activated BN ribbon.

Figure 4 illustrates the nitrogen adsorption/desorption isotherm and the corresponding pore size distribution of the activated BN. The measured isotherm and hysteresis loop (Figure 4a) can closely be classified as the I and H4 types[21] according to the IUPAC nomenclature. The isotherm and hysteresis loop indicate that the activated BN is microporosity as well as contain slit-shaped mesopores that are associated with capillary condensation[28,29]. Therefore, the pore size distributions (PSD) were calculated in the framework of non-local density functional theory (NLDFT) method. A high surface area of 2078 m^2/g and high pore volume of 1.66 cm^3/g could be determined, respectively. Additionally the observed broad PSD exhibits a multimodal distribution with three main characteristic pore sizes of ~ 1.3, ~ 2.7, and ~ 3.9 nm[30], as shown in Figure 4b. We believe that the three different porous structures in the activated BN are from different gaseous group eliminations during the thermal decomposition of the activated BN precursor. It should be noted that the porous BN we synthesized in Ref. 18 displays only two main characteristic pore sizes of ~ 1.3 and ~ 3.9 nm. These results suggest that the P123 introduced into the precursor during the synthetic process is highly valuable to improve the surface area and change the porous structures.

Removal of metallic ions from water. The activated BN possesses large void spaces, numerous hydroxyl and organics groups, large pore volume and structural defects. Combining these characteristics with the dipolar nature of B-N bonds renders the activated BN highly preferred for removal of environmental pollutants as an universal absorption material[15]. Indeed, we observed the excellent adsorption performance of the activated BN for Cr (III) in water.

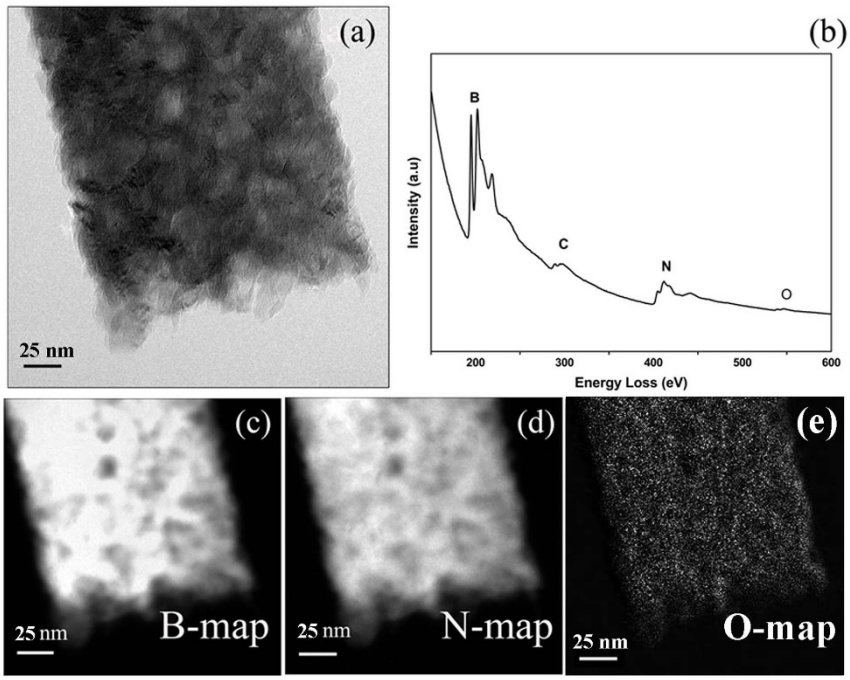

Figure 3 | (a) Energy filtering TEM (EFTEM) image (Zero-loss image) of a single ribbon. (b) The corresponding EEL spectrum. (c–e) Elemental mapping for B, N, and O, respectively.

High dispersion inductively couple plasma emission spectroscopy was employed to assess the adsorption kinetics. An activated BN sample of 50 mg was used to room-temperature absorb Cr (III) aqueous solution with the initial concentration of 52 mg/L and the optimum initial pH value of 5.5[7,31]. Shown in Figure 5a, we found the extremely rapid adsorption rate of 90 wt% within 4 h and 99.9 wt% within 6 h. The adsorption equilibrium concentration *vs* adsorbed amount well follows the Langmuir mode with a correlation coefficient of 0.991 (Figure 5b). The maximum adsorption capacity of Cr (III) in the activated BN is extremely high up to 352 mg/g, which corresponds to complete monolayer coverage. This value is much higher than the reported absorption of Cr (III) using activated carbon as a adsorbent (40.29 mg/g)[32]. More importantly, the final equilibrium concentration is only 0.052 mg/L (52 ppb), below the drinking water guideline in USA (100 ppb). We also studied the adsorption capacities of activated BN for other metal ions in water, including Co^{2+}, Ni^{2+}, Ce^{3+} and Pb^{2+}, as shown in Figure 5c. The detected maximum uptake capacities of Co^{2+}, Ni^{2+}, Ce^{3+}, and Pb^{2+} are as high as 215, 235, 282 and 225 mg/g, respectively. For comparsion, the adsorption capacities of porous BN (synthesized in Ref. 18) and activated carbon for these metal ions are also shown in Figure 5c. It clearly indicates that the maximum uptake capacities of activated BN are significantly larger than that of the porous BN and activated carbon reported in the literatures[33–36]. We believe that different from the activated carbon with covalent C-C bonds, our activated BN with polar B-N bonds is more suitable for the metal ion chemisorption, since the activated BN exhibits the "lop-sided" densities characteristic of ionic B-N bonding, and the polyelectron nitride can transfer more electron density to the metal ions. Moreover, the exceptional high surface area and abundant inter accommodations in the activated BN also play an important role in the high adsorption capacity and efficiency.

Removal of organic pollutant from aqueous environment. In addition, organic pollutant containing aromatic species in the source of drinking water has provided a more serious threat to human health than others. The removal of tetracycline, one of the most commonly used antibiotics in the husbandry and fish farming, faces an immense technical challenge especially in the developing countries. The activated BN reported here surprisingly exhibits a remarkable adsorption capacity for tetracycline. Its adsorption isotherm is presented in Figure 6a, again revealing that the

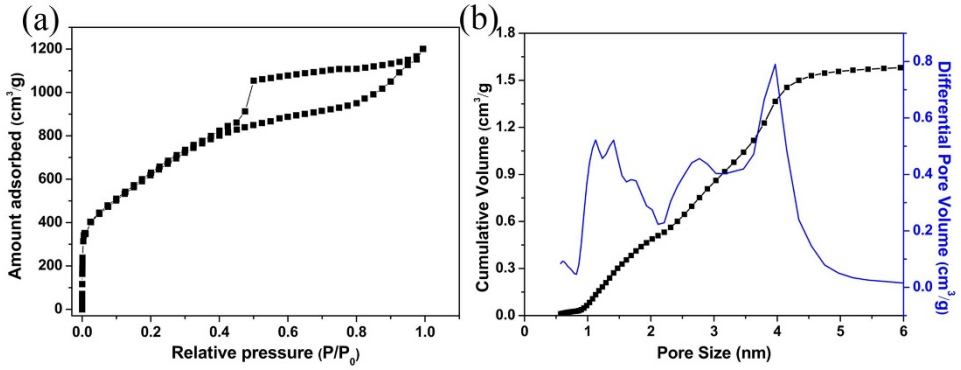

Figure 4 | (a) Nitrogen adsorption/desorption isotherm. (b) the corresponding pore size distributions obtained by DFT method (full line) and cumulative pore size distribution (square symbol).

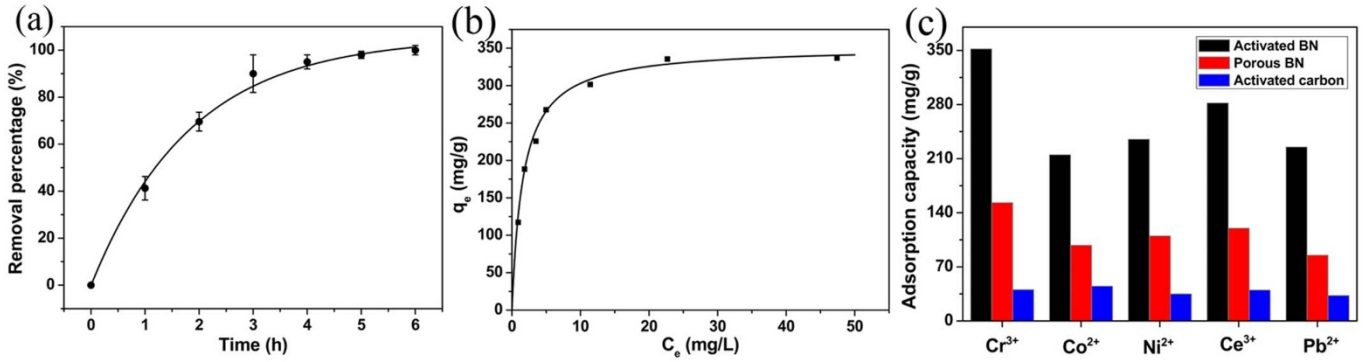

Figure 5 | (a) Adsorption rate of trivalent chromium ions on the activated BN. (b) The corresponding adsorption isotherm. (c) Comparison of adsorption capacities of the activated BN, porous BN and activated carbon for Co^{2+}, Ni^{2+}, Ce^{3+}, and Pb^{2+}, respectively.

Langmuir model well fits with the experimental data with the correlation coefficient of 0.998. The adsorbed layer is one molecule in thickness and all sites are equal (equal energies and enthalpies). The maximum adsorption capacity obtained is 305 mg/g for the activated BN. This value is remarkably larger than that of most of the reported adsorbents[37,38], including multi-walled carbon nanotubes (56.5 mg/g), activated carbon (25.2 mg/g) and porous BN (176.8 mg/g). We also note that the adsorption curve (Figure 6a) for the activated BN has a very high slope in the initial portion and then level off. This result reveals that the activated BN possesses incredible adsorption density even at low equilibrium organic pollutant concentrations and displays very high affinity for tetracycline molecules. More importantly, the as-adsorbed activated BN can be easily regenerated by a simple thermal treatment route at 400°C for 2 h in air. All adsorbate were removed without any loss of the BN. The repeated measurement for the tetracycline adsorption indicates only ~ 14% efficiency loss after six cycles, as presented in Figure 6b. Keeping in mind of excellent reusability and safety, the titled material is suitable for lowering organic pollutant concentration in the source of drinking water. Figure 6c shows a comparison of removal capacities of activated BN, porous BN, and activated carbon for tetracycline, methyl orange and congo red, respectively. The data suggest excellent adsorption capacity in our newly prepared activated BN material.

Adsorption of volatile organic compounds in air. We also hope that the activated BN is able to use in another interesting environment purification field, to adsorb volatile organic gas molecules in air. Herein, as a demonstration we report its adsorption to benzene vapor. Gravimetric adsorption measurements, similar with the reported method for the vapor adsorption of activated carbon[39], were carried out. The activated BN was introduced into a container full of the saturate benzene vapor at room temperature. The starting dry BN became humid after vapor adsorption. Figure 7a shows adsorption rate of benzene vapors on activated BN at different time intervals. The adsorption capacity was measured to be 90 mg/g within 1 h, and reached 762.5 mg/g within 72 h, much higher than most of the adsorbents, including activated carbon (280 mg/g)[40,41] and porous BN (380 mg/g). The above experimental data indicate that the activated BN is suitable for fast and efficient air-purification. In order to further assess the practical air-purification potential for volatile organic species, a filtration column was prepared to test the breakthrough curve of benzene vapor, as a model pollutant, on the activated BN. Compared with the breakthrough curves of porous BN and activated carbon obtained under the same experimental condition, the benzene vapor could be removed completely within 100 min. This time is remarkably longer than that of porous BN and activated carbon, as summarized in Figure 7b. It is obvious that, for a given concentration of benzene vapor, the longer breakthrough time indicates a greater adsorption capacity. The reusability was also checked by direct calcinations of the as-measured BN at 300°C for 6 h in N_2 flow and then repeated measurement in the same condition. As shown in Figure 7c, the removal efficiency is still maintained ~ 95.5% even after six cycles.

As a comparison, non-porous BN particles (spherical BN particles with the surface are of ~ 50 m^2/g[23]) are examined under the same experimental condition. Only ~ 60 mg/g uptake after 72 h was detected (Figure 7a, inset) and suggests that the remarkable efficiency of the activated BN for volatile organic compounds in air similarly results from the large pore volume, high density structural defects, specific surface area[42,43], and numerous surface groups, as predicted theoretically[44]. In fact, the special structure of micro/meso- pore can

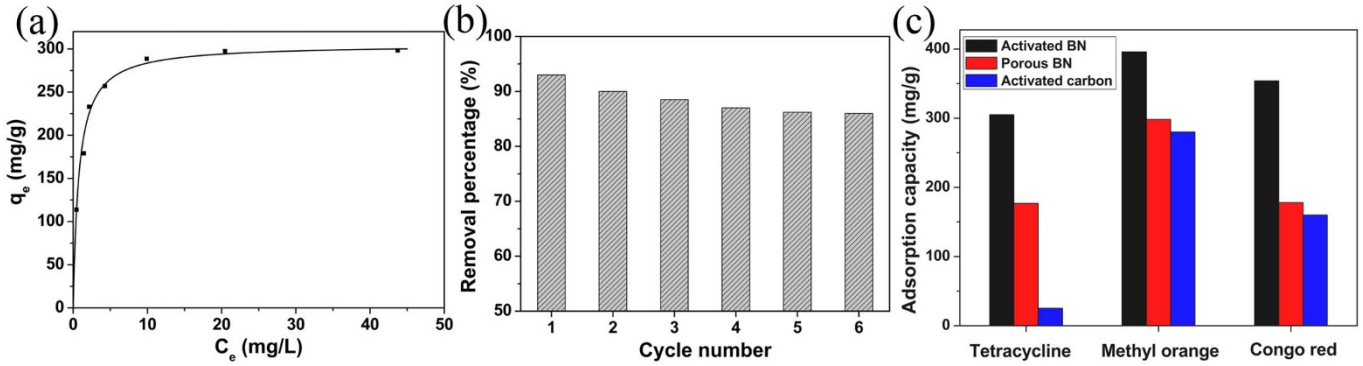

Figure 6 | (a) Adsorption isotherm of tetracycline on the activated BN. (b) Reusability of activated BN regenerated by combustion of adsorbed tetracycline. (c) Comparison of adsorption capacities of the activated BN, porous BN, and activated carbon for the tetracycline, methyl orange and congo red, respectively.

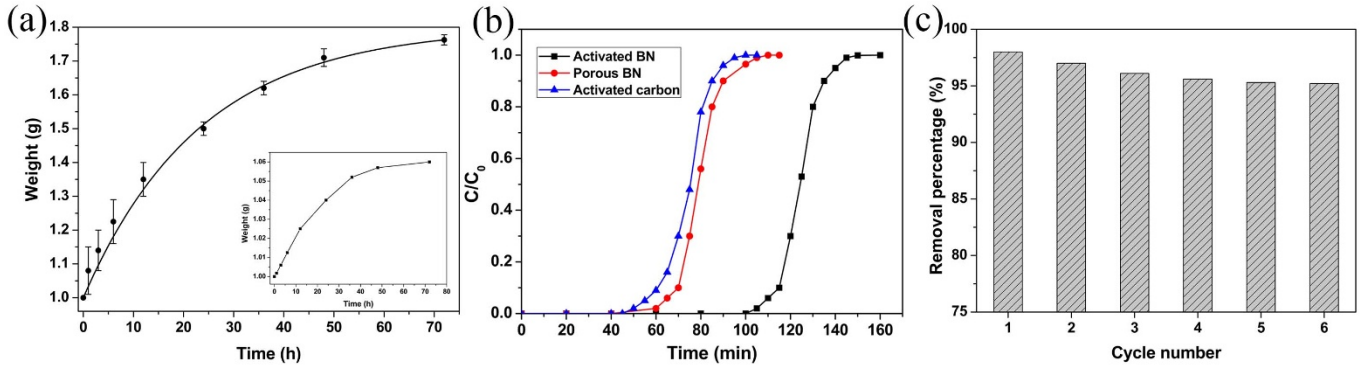

Figure 7 | (a) Adsorption rate of benzene vapor on the activated BN. (Inset) adsorption rate of benzene vapor on the non-porous BN. (b) Comparison of the breakthrough curve of benzene vapor on the filtration column of activated BN, porous BN and activated carbon, respectively. (c) Reusability of the activated BN regenerated by heating adsorbed benzene.

effectively enhance the benzene adsorption capacity, which has been frequently confirmed in the case of activated carbons[45,46].

Discussion

The above mentioned results reveal that, compared with the synthesis process for porous BN[18], the addition of P123 surfactant in this work not only increases the surface area and pore volume but also enhances the adsorption ability of the titled BN. Although the P123 was removed from the as-growth activated BN, which has been confirmed by the EEL spectrum, the interaction of P123 with the melamine-boric acid molecules affects the surface chemical configuration of the precursor of activated BN. As reported by Roy et al.[47], the melamine-boric acid molecular crystal contained several kinds of hydrogen bonds, such as O-H···O, N-H···O, and O-H···N. One of the amino groups of melamine did not participate in hydrogen bonding in the melamine-boric acid molecule. Therefore, the addition of P123 would lead to the hydrogen-bonding between the melamine and P123 molecule in the precursor. This would result in the formation of more gaseous groups during the post-treatment at high temperature, such as H_2O, NH_3, N_2 and CO. These gaseous groups were removed through the spaces between layers or other positions located by these groups, and a larger number of porosities were finally obtained. The TG-DTA curves also indicate an obvious weight loss occurred during the heating treatment of the precursor (See Figure S1, Supporting Information). This synthetic route might promote the generation of some useful surface groups, the variation of pore structure, and the enhancement of surface area and pore volume[5,48], which is suitable for the adsorption of metallic ions, organic pollutants and gaseous species. The detailed mechanism is worthy of further investigation.

In summary, highly activated boron nitride has successfully been synthesized by introducing structure-directed agent in a process of the thermal decomposition of the activated BN precursor. The obtained BN with rich surface groups possesses extremely high surface area (up to 2078 m^2/g), large pore volume (up to 1.66 cm^3/g), and a special multimodal microporous/mesoporous structure with three main characteristic pore sizes of ~ 1.3, ~ 2.7, and ~ 3.9 nm. Pore size design and targeted preparation by introducing structure-directed agent P123 represent a novel method for developing activated BN. More importantly, the activated BN exhibits an excellent adsorption performance for metal ions and organic pollutant in water, as well as volatile organic species in air. The excellent reusability of activated BN has also been confirmed. All the features render the activated BN a promising material suitable for environmental remediation.

Methods

Synthesis. In a typical synthesis, 3.71 g of H_3BO_3 and 3.78 g of $C_3N_6H_6$ were dissolved in 200 ml of the distilled water. Then 0.1 M HNO_3 solution was introduced to achieve a solution with pH of 6.5. 5 g of P123 (P123 is the tradename for a triblock copolymer. The nominal chemical formula is $HO(CH_2CH_2O)_{20}(CH_2CH(CH_3)O)_{70}(CH_2CH_2O)_{20}H$. Triblock copolymers based on poly(ethylene glycol)-poly(propylene glycol)-poly(ethylene glycol) are known generically as poloxamer and have been used in the synthesis of porous materials.) was added under vigorous stirring to get a homogenous solution. The reaction mixtures were heated at 85°C for 6 h, and then naturally cooled to room temperature to obtain a white precipitate, melamine-boric acid molecule precursor. After the filtration, the precursor was washed with chilled de-ionized water and dried at 90°C for 12 h. Subsequently, a two-stage pyrolytic process was performed to produce the activated BN: the precursors were calcined at 546°C for 2 h and then heated at 1300°C for 8 h. All the reactions were carried out in a flow of N_2 (200 ml/min).

Adsorption/desorption in water. $CrCl_3$, $CoCl_2$, $Pb(NO_3)_2$, $Ce(NO_3)_3$, $Ni(NO_3)_2$, $C_{22}H_{24}N_2O_8S_3Na_2$ (methyl orange), and $C_{32}H_{22}N_6Na_2O_6S_2$ (congo red) were dissolved in deionized water and then diluted to the required concentration before use. The pH values of initial solutions were adjusted from 5.0 to 6.0 (5.5 for Cr(III), 6.0 for Pb(II), 6.0 for Ce(III), 6.0 for Co(II), 6.0 for Ni(II), 6.0 for tetracycline, and 7.0 for methyl orange, congo red) by adding 0.1 M HNO_3 solution, respectively. Then the as-synthesized activated BN, the porous BN and the activated carbon were introduced and continuously stirred by a magnetic stirrer at 150 rpm for a specified time, and then centrifuged and filtered, repectively. The solution concentrations were determined by high dispersion inductively couple plasma emission spectroscopy and UV/vis spectrophotometer, respectively. To obtain the isotherms, the adsorption tests were carried out with a series of initial concentrations. The pollutant removal percentage over the adsorbent was calculated by the Eq. 1

$$\eta(\%) = (C_0 - C_e)\cdot 100/C_0 \quad (1)$$

where C_0 and C_e (mg/L) are the initial solution concentration and equilibrium concentration, respectively. η is the pollutant removal percentage of the pollutants.

The adsorption isotherms are fitted (correlation coefficients, $R^2 > 0.99$) by using the Langmuir adsorption model (Eq. 2).

$$q_e = q_m K C_e/(1 + K C_e) \quad (2)$$

Where q_e is the adsorbed amount of pollutant on the equilibrium concentration (mg/g), C_e is the equilibrium concentration in solution (mg/L), q_m is the maximum adsorption capacity corresponding to complete monolayer covering on the adsorbents (mg/g), and K is the equilibrium constant related to the free energy of adsorption (L/mg).

Benzene vapor adsorption. The activated BN powder was introduced into a container full of benzene vapor to measure its gravimetric change at room temperature. The breakthrough curve of benzene vapor was obtained by using the activated BN filtration column (25 mm height and 40 mm internal diameter), which was prepared by a filtration column loaded with 3 g activated BN. The measurement conditions were optimized as the relative humidity 50%, temperature 23°C, inlet concentration 18 mg/L, and a constant flow rate 0.25 L/min.

Characterization. The structure and morphology of the samples were examined using X-ray powder diffraction (XRD, BRUKER D8 FOCUS) and field emission scanning electron microscopy (SEM, HITACHI S-4800). FTIR spectra recorded on a Nicolet 7100 spectrophotometer between 400 and 4000 cm^{-1}. Transmission electron microscopy (TEM) experiments were performed on a Tecnai F20 electron microscope (Philips, Netherlands) with an acceleration voltage of 200 kV, equipping with an electron energy loss spectrometer (EELS). Thermogravimetry (TG) and differential thermal analysis (DTA) were measured on a SDTQ-600 thermal analyzer from room temperature to 1200°C at a heating rate of 10°C/min under nitrogen flow. The nitrogen physisorption isotherms were measured at 77 K on an AutoSorb iQ-C

TCD analyzer. Prior to the measurement, the samples were activated in vacuum at 300°C for 8 h. The Brunauer-Emmett-Teller (BET) specific surface area was calculated from the nitrogen adsorption data in the relative pressure ranging from 0.02 to 0.12 using a multipoint BET method. Due to the broad pore size distribution ranging from micropores to mesopores, the NLDFT method was used to calculate the pore widths and pore size distributions (ASiQwin software). In detail, a set of isotherms calculated for a set of pore sizes in a given range for a given adsorptive constitutes the model database. Such a set of isotherms, called a kernel, is the basis for the pore size analysis by Density Functional Theory (DFT). The calculation of the pore size distribution is based on a solution of the Generalized Adsorption Isotherm (GAI) equation, which correlates the kernel of theoretical adsorption/desorption isotherms with the experimental sorption isotherm. Concentrations of metal ions were measured by high dispersion inductively couple plasma emission spectroscopy (TELEDYNE-Leeman Labs, USA). A double beam UV/Vis spectrophotometer (HITACHI, U-3900H) was used to determine the concentration of tetracycline. Benzene vapor concentration was determined by gas chromatograph (PGENERAL, GC1100).

1. Shannon, M. A. *et al*. Science and technology for water purification in the coming decades. *Nature* **452**, 301–310 (2008).
2. Montgomery, M. A. & Elimelech, M. Water and sanitation in developing countries: including health in the equation. *Environ. Sci. Technol.* **41**, 17–24 (2007).
3. Zhang, F. *et al*. Nanowire-Haired Inorganic Membranes with Superhydrophilicity and Underwater Ultralow Adhesive Superoleophobicity for High-Efficiency Oil/Water Separation. *Adv. Mater.* DOI:10.1002/adma.201301480 (2013).
4. Brooks, A. J., Lim, H. N. & Kilduff, J. E. Adsorption uptake of synthetic organic chemicals by carbon nanotubes and activated carbons. *Nanotech.* **23**, 294008 (2012).
5. Liu, Y. B. *et al*. Synthesis of high saturation magnetization superparamagnetic Fe_3O_4 hollow microspheres for swift chromium removal. *ACS Appl. Mater. Interfaces* **4**, 4913–4920 (2012).
6. Liang, H. W. *et al*. Robust and highly efficient free-standing carbonaceous nanofiber membranes for water purification. *Adv. Funct. Mater.* **21**, 3851–3858 (2011).
7. Deng, S. B. & Bai, R. B. Removal of trivalent and hexavalent chromium with aminated polyacrylonitrile fibers: performance and mechanisms. *Water Res.* **38**, 2424–2432 (2004).
8. Paine, R. T. & Narula, C. K. Synthetic routes to boron nitride. *Chem. Rev.* **90**, 73–91 (1990).
9. Pattanayak, J., Kar, T. & Scheiner, S. J. Boron−Nitrogen (BN) Substitution of Fullerenes: C_{60} to $C_{12}B_{24}N_{24}$ CBN. *Ball. Phys. Chem. A* **106**, 2970–2978 (2002).
10. Zhi, C. Y., Bando, Y., Tang, C. C., Kuwahara, H. & Golberg, D. Large-scale fabrication of boron nitride nanosheets and their utilization in polymeric composites with improved thermal and mechanical properties. *Adv. Mater.* **21**, 2889–289 (2009).
11. Meng, X. L. *et al*. Simple synthesis of mesoporous boron nitride with strong cathodoluminescence emission. *J. Solid State Chem.* **184**, 859–862 (2011).
12. Perdigon-Melon, J. A., Auroux, A., Guimon, C. & Bonnetot, B. J. Micrometric BN powders used as catalyst support: influence of the precursor on the properties of the BN ceramic. *J. Solid State Chem.* **177**, 609–615 (2004).
13. Borovinskaya, I. P., Bunin, V. A. & Merzhanov, A. G. Self-propagating high-temperatrue synthesis of high-porous boron nitride. *Mendeleev Commun.* **7**, 47–48 (1997).
14. Tang, C. C., Bando, Y., Ding, X. X., Qi, S. R. & Golberg, D. Catalyzed collapse and enhanced hydrogen storage of BN nanotubes. *J. Am. Chem. Soc.* **124**, 14550–14551 (2002).
15. Lian, G. *et al*. Ccontrolled fabrication of ultrathin-shell BN hollow spheres with excellent performance in hydrogen storage and wastewater treatment. *Energ. Environ. Sci.* **5**, 7072–7080 (2012).
16. Zhi, C. Y., Bando, Y., Terao, T. S., Tang, C. & Golberg, D. Dielectric and thermal properties of epoxy/boron nitride nanotube composites. *Pure Appl. Chem.* **82**, 2175–2183 (2010).
17. Zhi, C. Y., Hanagata, N., Bando, Y. & Golberg, D. Dispersible shortened boron nitride nanotubes with improved molecule loading capacity. *Chem. Asian J.* **6**, 2530–2535 (2011).
18. Li, J. *et al*. Porous boron nitride with a high surface area: hydrogen storage and water treatment. *Nanotech.* **24**, 155603 (2013).
19. Sun, Q. *et al*. Charge-controlled switchable CO_2 capture on boron nitride nanomaterials. *J. Am. Chem. Soc.* **135**, 8246–8253 (2013).
20. Lei, W. W., Portehault, D., Liu, D., Qin, S. & Chen, Y. Porous boron nitride nanosheets for effective water cleaning. *Nat. Commun.* DOI: 10.1038/ncomms2818 (2013).
21. Weng, Q. H. Preparation and hydrogen sorption performances of BCNO porous microbelts with ultra-narrow and tunable pore widths. *Chem. Asian J.* DOI: 10.1002/asia.201300940 (2013).
22. Han, W. Q., Brutchey, R., Tilley, T. D. & Zettl, A. Activated boron nitride derived from activated carbon. *Nano Lett.* **4**, 173–176 (2004).
23. Tang, C. C., Bando, Y., Huang, Y., Zhi, C. Y. & Golberg, D. Synthetic routes and formation mechanisms of spherical boron nitride nanoparticles. *Adv. Funct. Mater.* **18**, 3653–3661 (2008).
24. Weng, Q. H., Wang, X. B., Zhi, C. Y., Bando, Y. & Golberg, D. Boron nitride porous microbelts for hydrogen storage. *ACS Nano* **7**, 1558–1565 (2013).
25. Zhi, C. Y., Bando, Y., Tang, C. C. & Golberg, D. Phonon characteristics and cathodolumininescence of boron nitride nanotubes. *Appl. Phys. Lett.* **86**, 213110 (2005).
26. Chen, Z. G. *et al*. Novel boron nitride hollow nanoribbons. *ACS Nano* **2**, 2183–2191 (2008).
27. Huang, Y. *et al*. Bulk synthesis, growth mechanism and properties of highly pure ultrafine boron nitride nanotubes with diameters of sub-10 nm. *Nanotech.* **22**, 145602 (2011).
28. Evans, R. & Tarazona, P. Theory of condensation in narrow capillaries. *Phys. Rev. Lett.* **52**, 557–560 (1984).
29. Schlienger, S. *et al*. Micro-, mesoporous boron nitride-based materials template for zeolites. *Chem. Mater.* **24**, 88–96 (2012).
30. Groen, J. C., Peffer, L. A. A. & Pérez-Ramírez, J. Pore size determination in modified micro- and mesoporous materials. Pitfalls and limitations in gas adsorption data analysis. *Micropor. Mesopor. Mater.* **60**, 1–17 (2003).
31. Wu, D. Y. *et al*. Revoval of trivalent chromium from aqueous solution by zeolite synthesized from coal fly ash. *J. Hazard. Mater.* **155**, 415–423 (2008).
32. Mohan, D., Singh, K. P. & Singh, V. K. Trivalent chromium removal from wastewater using low cost activated carbon derived from agricultural waste material and activated carbon fabric cloth. *J. Hazard. Mater.* **B135**, 280–295 (2006).
33. Shen, W. Z. *et al*. The effect of activated carbon fiber structure and loaded copper, cobalt, silver on the adsorption of dichloroethylene. *Colloids Surf. A.* **273**, 147–153 (2006).
34. Krishnan, K. A., Sreejalekshmi, K. G. & Baiju, R. S. Nickel(II) adsorption onto biomass based activated carbon obtained from sugarcane bagasse pith. *Bioresour. Technol.* **102**, 10239–10247 (2011).
35. Sumathi, S., Bhatia, S., Lee, K. T. & Mohamed, A. R. Cerium impregnated palm shell activated carbon (Ce/PSAC) sorbent for simultaneous removal of SO^2 and NO—Process study. *Chem. Eng. J.* **162**, 51–57 (2010).
36. Momčilović, M., Purenović, M., Bojić, A., Zarubica, A. & Ranđelović, M. Removal of lead(II) ions from aqueous solutions by adsorption onto pine cone activated carbon. *Desalination* **276**, 53–59 (2011).
37. Ji, L. L., Chen, W., Duan, L. & Zhu, D. Q. Mechanisms for strong adsorption of tetracycline to carbon nanotubes: A comparative study using activated carbon and graphite as adsorbents. *Environ. Sci. Technol.* **43**, 2322–2327 (2009).
38. Wang, F., Zhu, D. Q. & Chen, W. Effect of copper ion on adsorption of chlorinated phenols and 1-naphthylamine to surface-modified carbon nanotubes. *Environ. Toxicol. Chem.* **31**, 100–107 (2012).
39. Foster, K. L., Fuerman, R. G., Economy, J., Larson, S. M. & Rood, M. J. Adsorption characteristics of trace volatile organic compounds in gas streams onto activated carbon fibers. *Chem. Mater.* **4**, 1068–1073 (1992).
40. Huang, Z. H., Kang, F. Y., Zheng, Y. P., Yang, J. B. & Ling, K. M. Adsorption of trace polar methy-ethyl-ketone and non-polar benzene vapors on viscose rayon-based activated carbon fibers. *Carbon* **40**, 1363–1367 (2002).
41. Liu, P. *et al*. Adsorption of trichloroethylene and benzene vapors onto hypercrosslinked polymeric risin. *J. Hazard. Mater.* **166**, 46–51 (2009).
42. Hu, Y. H. & Zhang, L. Hydrogen storage in metal-organic frameworks. *Adv. Mater.* **22**, E117–E130 (2010).
43. Lin, Y. C., Yan, Q. J., Kong, C. L. & Chen, L. Polyethyleneimine lncorporated metal-organic frameworks adsorbent for highly selective CO_2 capture. *Sci. Rep.* **3**, 1859; DOI:10.1038/srep01859 (2013).
44. Li, Y. F., Zhou, Z., Shen, P. W., Zhang, S. B. & Chen, Z. F. Computational studies on hydrogen storage in aluminum nitride nanowires/tubes. *Nanotech.* **20**, 215701 (2009).
45. Sircar, S. Capillary condensation theory for adsorption of vapors on mesoporous solids. *Surf. Sci.* **164**, 393–402 (1985).
46. Cal, M. P., Rood, M. J. & Larson, S. M. Removal of VOCs from humidified gas streams using activated carbon cloth. *Gas. Sep. Purif.* **10**, 117–121 (1996).
47. Roy, A., Choudhury, A. & Rao, C. N. R. Supramolecular hydrogen-bonded structure of a 2 : 1 adduct of melamine with boric acid. *J. Mol. Struct.* **613**, 61–66 (2002).
48. Deng, H. *et al*. Monodisperse magnetic single-crystal ferrite microspheres. *Angew. Chem. Int. Ed.* **44**, 2782–2785 (2005).

Acknowledgments

The authors are grateful to Dr. Y. H. Ma and J. Zhang for experimental support. This work was supported by the National Natural Science Foundation of China (51372066, 51172060, 51202055, 21103056), the National Basic Research Program of China (973 Programs: 2011CB612301), the Natural Science Foundation of Hebei Province (Grant No. E2012202040), and the Innovation Fund for Excellent Youth of Hebei Univeristy of Technology (No.2012001). The authors acknowledge the facilities, and the scientific and technical assistance of the Australian Microscopy & Microanalysis Research Facility at the Centre for Microscopy and Microanalysis, The University of Queensland.

Author contributions

L.J. and T.C. conceived and designed the experiments. L.J., X.X., X.W.X. and X.Y. performed the experiments and analyzed the data. Y.H. and J.Z. preformed the TEM

characterization. L.J., T.C., L.J. and J.P. wrote the manuscript. All authors discussed and commented on the manuscript.

Additional information

Supplementary information accompanies this paper at http://www.nature.com/scientificreports

Competing financial interests: The authors declare no competing financial interests.

How to cite this article: Li, J. *et al.* Activated boron nitride as an effective adsorbent for metal ions and organic pollutants. *Sci. Rep.* **3**, 3208; DOI:10.1038/srep03208 (2013).